ELSEVIER

Journal of Wind Engineering
and Industrial Aerodynamics 96 (2008) 1616–1628

JOURNAL OF wind engineering AND industrial aerodynamics

www.elsevier.com/locate/jweia

Application of generalized Richardson extrapolation to the computation of the flow across an asymmetric street intersection

J. Franke*, W. Frank

Department of Fluid and Thermodynamics, University of Siegen, Siegen, Germany

Available online 3 June 2008

Abstract

The validation of simulation results obtained from computational fluid dynamics (CFD) requires the estimation of the errors resulting especially from the spatial discretisation in space when steady solutions are computed. In this paper spatial discretisation errors are estimated with generalized Richardson extrapolation for the three mean velocity components at measurement positions within an asymmetric street intersection. The computational solutions are obtained with the code FLUENT V6.1 by solving the Reynolds averaged Navier–Stokes equations together with the standard k–ε turbulence model. From the solutions on five grids two grid triplets are formed, one with a constant refinement ratio of two and one with a smaller, nearly constant refinement ratio. From both grid triplets error estimates are possible for approximately 70% of the measurement locations. The resulting error bands agree fairly well, although the grid triplet with constant refinement ratio uses solutions from a substantially coarser grid than the triplet with non-constant refinement ratio. This fact is, however, correctly reflected by the larger error bands obtained for the grid triplet with the coarse grid solution which is most likely not in the asymptotic range.

Keywords: Urban flow; Street intersection; RANS; Standard k–ε model; Solution verification; Generalized Richardson extrapolation

*Corresponding author at: Institut für Fluid- und Thermodynamik, Universität Siegen, Paul-Bonatz-Strasse 9-11, D-57076 Siegen, Germany. Tel.: +49 271 740 4683; fax: +49 271 740 2666.
E-mail address: franke@ift.mb.uni-siegen.de (J. Franke).

0167-6105/$ - see front matter © 2008 Elsevier Ltd. All rights reserved.
doi:10.1016/j.jweia.2008.02.003

1. Introduction

The increasing application of computational fluid dynamics (CFD) in all fields of wind engineering aggravates the need for a rigorous evaluation of the codes and models to improve the confidence in their results. Verification and validation are the keywords in building confidence in CFD results in general (Oberkampf et al., 2004; Roy, 2005) and should therefore also be applied to computational wind engineering (CWE) predictions. While validation is used to assess the modelling errors through comparison with experimental data, solution verification deals with numerical errors in CFD results. Besides computer round-off and incomplete iterative convergence the spatial and temporal discretisation are the main source of the numerical error. For the estimation of the discretisation error Richardson extrapolation (Richardson, 1910, 1927) is normally used. The generalized Richardson extrapolation (Roache, 1998) has been successfully applied by Cadafalch et al. (2002) to several flow problems including turbulence, heat transfer and chemical reaction and was shown to yield in general reliable estimates of the error band. Contrary to that Eça and Hoekstra (2002) found a large scatter of the results when applied to a variety of flows, including the flow over a 2D hill and a backward facing step (Eça and Hoekstra, 2004). They showed that grid triplets are in general not enough to obtain a reliable estimate of the error band and recommend a least squares approach with more than three grids.

However, in this paper the procedure proposed by Eça and Hoekstra (2004) for grid triplets is applied to the flow field across an asymmetric street intersection to test its suitability for typical problems of CWE. The error bands for the three statistically steady velocity components are estimated at those locations where measurements are available from the CEDVAL database (Leitl, 2000). In the following first the procedure for estimating the error bands is introduced. Then the geometry of the street intersection is described together with the computational domain and the five grids that are used. After the presentation of the boundary conditions and numerical parameters of the simulations the results for the estimated error bands are shown. Finally, conclusions are drawn in Section 6.

2. Procedure for estimation of error bands

With generalized Richardson extrapolation the spatial discretisation error δ_i of any local or integral quantity on mesh i can be approximated as

$$\delta_i = f_i - f_{\mathrm{ex}} \approx g h_i^p, \tag{1}$$

when retaining only the first term in the power series expansion. Here, f_i is the computed solution on mesh i and h_i the characteristic grid spacing. The three unknowns in Eq. (1) are the exact solution f_{ex}, the observed or apparent order of accuracy p and the constant g, which all can be computed with the aid of solutions on two more grids. Based on the ratio of the solution changes, $R = (f_2 - f_1)/(f_3 - f_2)$, where index 1 refers to the fine, index 2 to the medium and index 3 to the coarse grid, the computational nodes are classified following Eça and Hoekstra (2004):

- $0 < R < 1$, monotonic convergence;
- $-1 < R < 0$, oscillatory convergence;

- $R<-1$, oscillatory divergence;
- $R>1$, monotonic divergence.

For the nodes with monotonic convergence p is computed iteratively from the implicit relation

$$p = \{\ln(1/R) - [\ln(r_{32}^p - 1) - \ln(r_{21}^p - 1)]\}/\ln(r_{21}) \tag{2}$$

with the refinement ratios $r_{21} = h_2/h_1$ and $r_{32} = h_3/h_2$. For $r_{21} = r_{32}$ the determination of the observed order of accuracy is simplified and p is calculated from the explicit relation $p = \ln(1/R)/\ln(r_{21})$. If the computed p is larger than the theoretical order, which is between one and two in the present work, the following relation for the error estimate δ_i' is solved with the grid triplet (Roy, 2003; Eça and Hoekstra, 2004).

$$\delta_i' = f_i - f_{ex} \approx g_1 h_i + g_2 h_i^2. \tag{3}$$

The numerical error band U_1 on the finest grid is estimated with the grid convergence index (GCI) as proposed by Roache (1994) and extended by Eça and Hoekstra (2004). In the case of monotonic convergence the estimate depends on the observed order of accuracy p.

- For $0.5<p\leqslant 2$

$$\text{(I)} \quad U_1 = 1.25|\delta_1|. \tag{4}$$

- For $2<p\leqslant 3$

$$\text{(II)} \quad U_1 = 1.25\max(|\delta_1|, |\delta_1'|). \tag{5}$$

- For $p\leqslant 0.5$ or $p>3$

$$\text{(III)} \quad U_1 = 3\max(|f_3 - f_2|, |f_2 - f_1|). \tag{6}$$

Eq. (6) is also used for the error band estimation ($\pm U_1$) in the case of oscillatory convergence, denoted by (IV). Finally, no error band estimate is made for the cases with oscillatory or monotonic divergence, or if the iterative solution of Eq. (2) does not converge or yields observed orders of accuracy of $p\leqslant 0$ or $p>10$. Eça and Hoekstra (2002) used $0<p<8$ as admissible range. All these four cases are denoted by (V) in the following.

3. Computational domain and grids for the asymmetric intersection

The asymmetric street intersection is formed by four ring shaped buildings of which two partially have a slanted roof, see Fig. 1(a). The height of the two buildings with flat roof is $H = 0.06\,\text{m}$, which is also the width of the streets. The asymmetry of the intersection results from shifting the rear buildings by H in positive y direction. The four buildings are placed in the block shaped computational domain shown in Fig. 1(b). The large distances from the built area have been chosen to render the influence of the boundary conditions on the flow inside the intersection as small as possible. The size of the domain fulfils the requirements given by Franke et al. (2004).

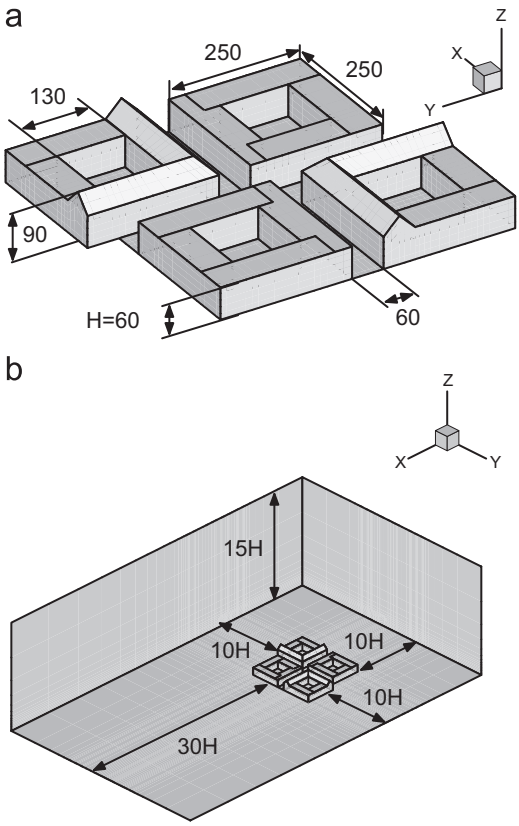

Fig. 1. (a) Geometry of the buildings and street canyons with all given sizes in mm and (b) size of the computational domain.

As explained above the application of generalized Richardson extrapolation requires solutions on three systematically refined or coarsened grids, which can be structured or unstructured, but must have a consistent grid refinement ratio in the entire domain (Roy, 2005). In the case of unstructured grids made of tetrahedral elements a refinement ratio of $r_{21} = r_{32} = 2$ is recommended (Roache, 1998; Roy, 2005). Starting with the coarsest grid the refined grids can then be generated by always dividing one tetrahedral element into eight small tetrahedral elements (Roy, 2005). For structured grids the opposite approach is recommended. From the finest grid the coarser grids are obtained by omitting every second grid line. In the general case of non-uniform grids the expansion ratios between consecutive grid intervals additionally have to be enlarged to obtain smooth coarsened meshes (Roache, 1998; Roy, 2005). This approach was also used in the present work.

Inside the computational domain altogether five block structured grids were generated with a consistent refinement ratio. The finest grid consists of 2 335 360 hexahedral cells with a cell height of 0.05 H on the ground floor. From this fine grid two coarser grids have been generated manually by omitting every second grid line and always doubling the cell height on the ground floor. The medium mesh consists of 291 920 hexahedral cells and the

coarse mesh of 36 490. With this approach for coarsening grids the expansion ratio between consecutive grid intervals cannot be kept constant. While for the fine mesh the maximum ratio of neighbouring cell sizes is below 2.05, it increases to 3.47 on the medium grid and to even 5.42 on the coarse grid. All these values correspond to substantially larger expansion ratios than the recommended maximum of 1.3 (Franke et al., 2004).

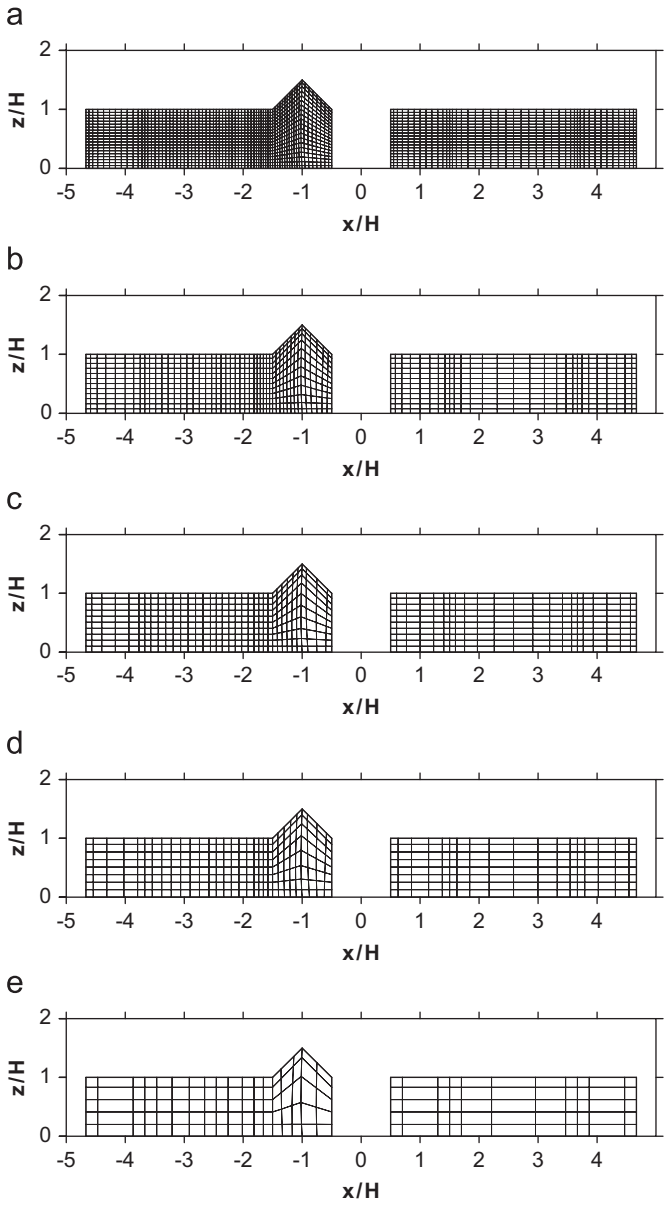

Fig. 2. Resolution of the buildings' height with the five grids: (a) fine, (b) medium of grid triplet B, (c) medium of grid triplet A, (d) coarse of grid triplet B and (e) coarse of grid triplet A.

Furthermore this approach does not lead to grids with coincident computational nodes on the coarse grid, which are necessary if Richardson extrapolation is to be used on the coarse grid nodes without interpolation of the solutions (Roache, 1998). As in this work Richardson extrapolation is performed at measurement positions which do not coincide with computational nodes, interpolation of the solution has to be used for all three grids, see Section 5.

The three grids described above form one grid triplet that is used in the generalized Richardson extrapolation described in Section 2. From the number of computational cells of each grid, N_i, the refinement ratio is calculated as $r_{i+1i} = (N_i/N_{i+1})^{1/3}$. For the grids

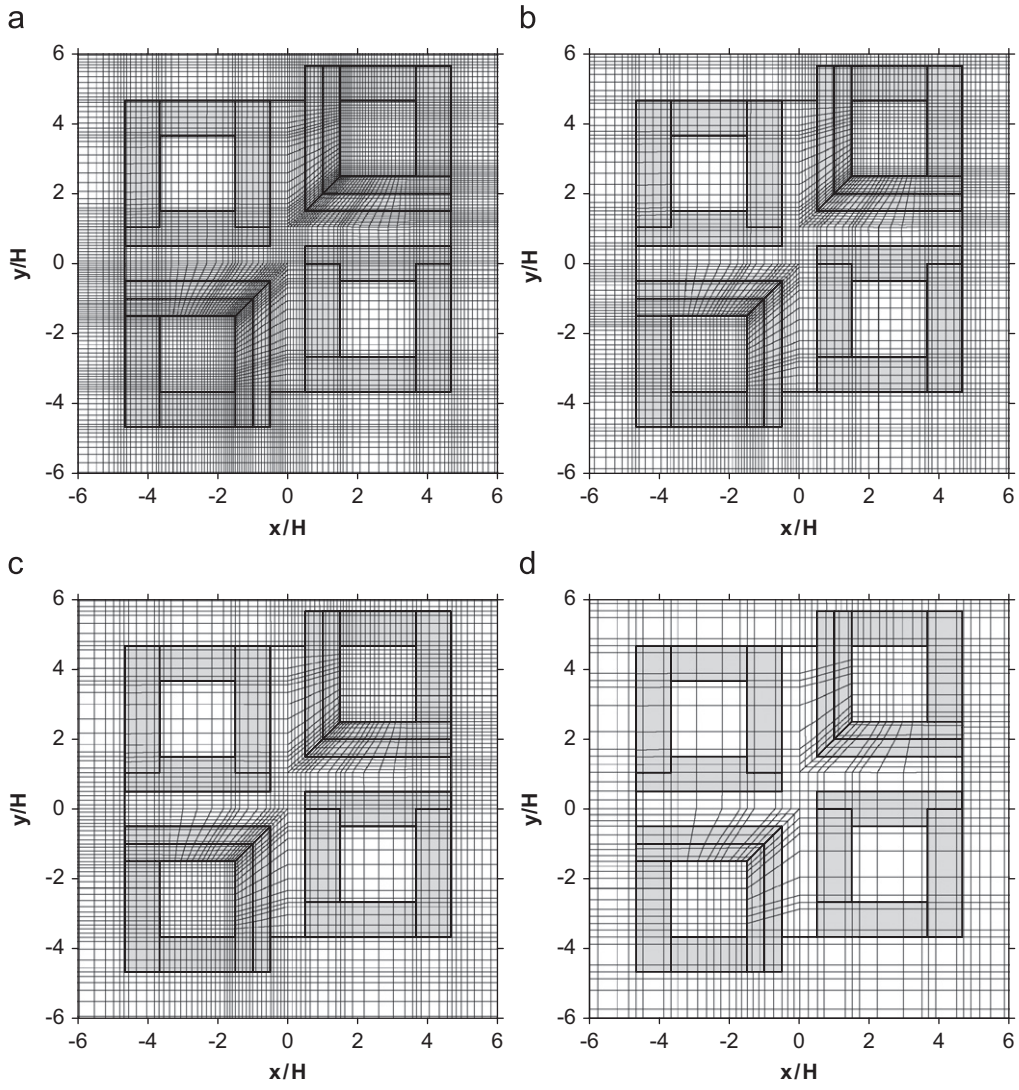

Fig. 3. Horizontal resolution of the built area: (a) medium of grid triplet B, (b) medium of grid triplet A, (c) coarse of grid triplet B and (d) coarse of grid triplet A.

described above the resulting ratios are equal, $r_{21} = r_{32} = 2$, and the observed order of accuracy p can be calculated explicitly. These three grids will be referred to as grid triplet A in the following.

In addition to triplet A, a second grid triplet is used for the generalized Richardson extrapolation described in Section 2. This triplet is referred to as grid triplet B. In this triplet the fine mesh is the same as the one used for triplet A. The medium and the coarse grid were generated from the fine mesh by always reducing the number of grid lines by approximately 36% and increasing the height of the first cell on the ground floor accordingly, yielding a nearly constant refinement ratio in the entire domain. The medium mesh contains 615 084 hexahedral cells and the coarse mesh 160 960. From the number of cells the corresponding refinement ratios follow as $r_{21} = 1.56006$ and $r_{32} = 1.56341$. Although the ratios are nearly equal, Eq. (2) must be used to calculate the observed order of accuracy p iteratively.

Concerning the maximum ratio of neighbouring cell sizes triplet B has the following charactersitics. For the medium mesh the maximum ratio is 1.84 and therefore even smaller than the corresponding value for the fine grid. For the coarse grid the maximum is 2.90. This can be also seen in Figs. 2 and 3, where details of the five grids are shown. Especially in Figs. 2(e) and 3(d) the large changes in cell size for the coarse mesh of triplet A are clearly visible.

4. Numerical parameters and boundary conditions

The flow field across the asymmetric street intersection has been computed by solving the Reynolds averaged Navier–Stokes (RANS) equations with the double precision version of the general purpose code FLUENT V6.1.22. For the generalized Richardson extrapolation only the results obtained with the standard k–ε turbulence model are used. The performance of other turbulence models and the comparison with experimental results is described by Franke and Frank (2005). The reason for choosing the results obtained with the standard k–ε model is its excellent monotonic convergence of the iterative solution of the algebraic system of equations on all five meshes. The scaled residuals (FLUENT, 2003) of all solution variables reached the iterative convergence criterion of 10^{-6}. In addition to the magnitude of the residuals the solution variables themselves were monitored at several measurement positions as function of the iterations to judge convergence. At the examined locations all variables were constant before the convergence criteria were reached.

As numerical approximation the second-order upwind interpolation was used for the convective terms of all solution variables. Derivatives were approximated in the cell centres (FLUENT, 2003). The theoretical order of accuracy of the approximations is therefore two on equidistant grids and between one and two for non-equidistant grids.

At the boundaries of the computational domain shown in Fig. 1(b) the following boundary conditions have been applied. At the outlet plane a constant pressure is prescribed and the normal derivatives of all other flow variables are forced to vanish. On the lateral sides and on the top symmetry boundary conditions are used. The walls of the buildings and the streets between the buildings are treated as smooth walls while a constant roughness is assigned to the ground floor around the buildings. At all walls the solution variables are computed with the standard wall function approach (FLUENT, 2003). As the rough wall functions in FLUENT are implemented in terms of the sandgrain roughness

k_s, the hydrodynamic roughness $z_0 = 0.4$ mm, which is provided in the CEDVAL database (Leitl, 2000), has to be converted into the sandgrain roughness. In the current simulations the relation $k_s = 30\ z_0 = 12$ mm $= 0.2$ H is used together with a value of $C_s = 0.5$ for the user defined constant in FLUENT's rough wall formulation (FLUENT, 2003). Therefore, the prescribed sandgrain roughness is larger than half of the cell height at the ground floor for all five grids. In this case FLUENT uses half of the cell height at the ground floor for k_s instead of the prescribed value, as we found from a careful analysis of a simple 2D equilibrium boundary layer flow over a rough wall. This means that the effective sandgrain roughness is different for every mesh.

Another consequence of the inconsistency between the roughness height and the cell height at the ground floor is, that the profiles for the velocity components and the turbulence quantities, which are prescribed at the inlet plane, change substantially within the computational domain until the built area is reached. While the u velocity component in x direction is only slightly decreased close to the ground, the turbulent kinetic energy k is substantially reduced up to a height of 2 H, as Franke and Frank (2005) have already shown at a distance of 5 H from the inflow plane. Similar results were recently presented by Blocken et al. (2007) for the atmospheric boundary layer in general. Like in the present work they used the equilibrium profiles proposed by Richards and Hoxey (1993) for the standard k–ε model in terms of the hydrodynamic roughness height z_0 of the ground floor as inflow boundary condition. These boundary conditions consist of a logarithmic distribution of the u velocity component as a function of height and a constant turbulent kinetic energy k.

Blocken et al. (2007) also point to the inconsistency between the inflow boundary conditions and the symmetry boundary condition at the top of the domain, as the equilibrium boundary layer profiles result from the assumption of a constant shear stress. Therefore the application of a constant shear stress at the top (Hargreaves and Wright, 2006) or the prescription of constant values for the velocity components and the turbulence quantities, derived from the inflow profiles at the height of top boundary, are consistent with the inflow boundary conditions (Blocken et al., 2007). For the present investigation, where generalized Richardson extrapolation requires the comparison of the different simulation results with each other, this inconsistency is not problematic as all solutions use the same top boundary condition. Furthermore the relatively small distance between the inflow plane and the built area and especially the large height of the domain reduce the influence of the symmetry condition at the top boundary on the results within the intersection.

5. Results

In Fig. 4, the measurement positions are shown. The 1691 measurement positions are grouped in two horizontal planes with constant z/H values and four vertical planes with constant y/H values. As the measurement positions do not coincide with the nodes of the grids interpolation is necessary for all grids. Linear interpolation within the commercial visualization software TECPLOT V10 has been used. As interpolations can negatively influence the results of grid convergence studies (Roache, 1998; Eça and Hoekstra, 2002, 2004; Roy, 2005), the linear interpolation results from TECPLOT V10 have been compared with results obtained using second, third and fourth-order interpolation within an in house code for the lid-driven cavity flow studied by Cadafalch

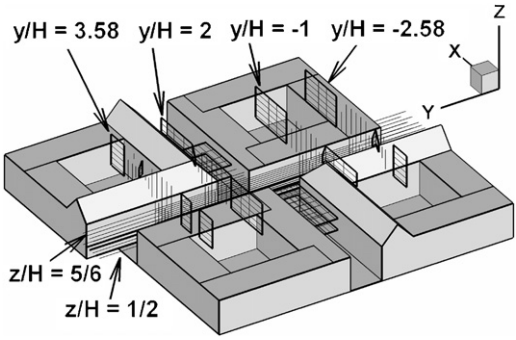

Fig. 4. Measurement locations, where the generalized Richardson extrapolation is performed.

Table 1
Grid convergence results for the flow across the asymmetric street intersection

Grid triplet	Variable	I (%)	II (%)	III (%)	IV (%)	V (%)	$\langle p \rangle$	p_{rms}	$\langle U_1 \rangle$ (%)	$U_{1,\mathrm{rms}}$ (%)
A	u	26.37	11.65	16.44	25.07	20.47	1.61	0.67	8.20	13.41
$r_{21} = r_{32} = 2$	v	21.70	9.70	18.39	25.19	25.02	1.58	0.70	14.62	19.00
	w	14.55	9.11	13.90	33.35	29.09	1.68	0.74	24.08	32.78
B	u	22.95	8.69	21.05	18.21	29.10	1.50	0.70	5.53	7.93
$r_{21} = 1.56006$	v	24.36	6.51	22.83	16.20	30.10	1.36	0.68	11.07	16.74
$r_{32} = 1.56341$	w	23.00	6.51	16.32	18.27	35.90	1.47	0.65	10.91	16.43

I, II, III, IV and V are the percentages of the 1691 measurement locations where the corresponding convergence criteria detailed in Section 2 are fulfilled. $\langle p \rangle$ is the mean observed order of accuracy computed for conditions I and II. p_{rms} is the corresponding RMS value. $\pm \langle U_1 \rangle$ is the average error band for conditions I–IV, normalized with the maximum magnitude of the corresponding variable value. $U_{1,\mathrm{rms}}$ is the corresponding RMS value, normalized in the same way.

et al. (2002) and for the 2D flow over a surface mounted beam (Franke and Frank, 2006). For these two cases the interpolation had only a minimal influence on the grid convergence analysis.

For both grid triplets defined in Section 3 every measurement location is classified in terms of the convergence criteria in dependence of the ratio of the solution changes, $R = (f_2 - f_1)/(f_3 - f_2)$, and the observed order of accuracy p, as defined in Section 2. In Table 1, the percentage of the locations falling into category I–V are listed for the three mean velocity components. For both grid triplets the u component has the smallest percentage of diverging conditions, where no estimate of the error band is made. The largest percentage of diverging positions is obtained for the w component. The differences are, however, small, with more diverging conditions obtained for triplet B with the non-constant refinement ratio. This increase of divergence is nearly entirely due to the fact that the iterative solution of Eq. (2) yields values for the observed order of accuracy outside the admitted range of $0 < p \leqslant 10$. The iterative solution failed only at five locations, four times for the u component and once for the w component. Concerning the oscillatory and the monotonic divergence, both contribute nearly equally to the total divergence.

For grid triplet A, a substantially larger number of positions displays oscillatory convergence IV than for triplet B. This might be attributed to the very coarse grid used in A because of the refinement ratio of two. The solution on the coarse grid is therefore most likely not in the asymptotic range, which is a necessary condition for Eq. (1) or (2) to be valid (e.g., Roache, 1998; Roy, 2005). On the other hand triplet B has a larger percentage of condition III as a result of the iterative determination of p. For conditions I and II both triplets give roughly the same result, except for the w component, where triplet B has more locations with monotonic convergence and observed orders of accuracy in the range $0.5 < p \leqslant 2$, condition I.

Also shown in Table 1 is the average order of accuracy $\langle p \rangle$ and its root mean square value, p_{rms}, which are computed from the results obtained for conditions I or II. Again

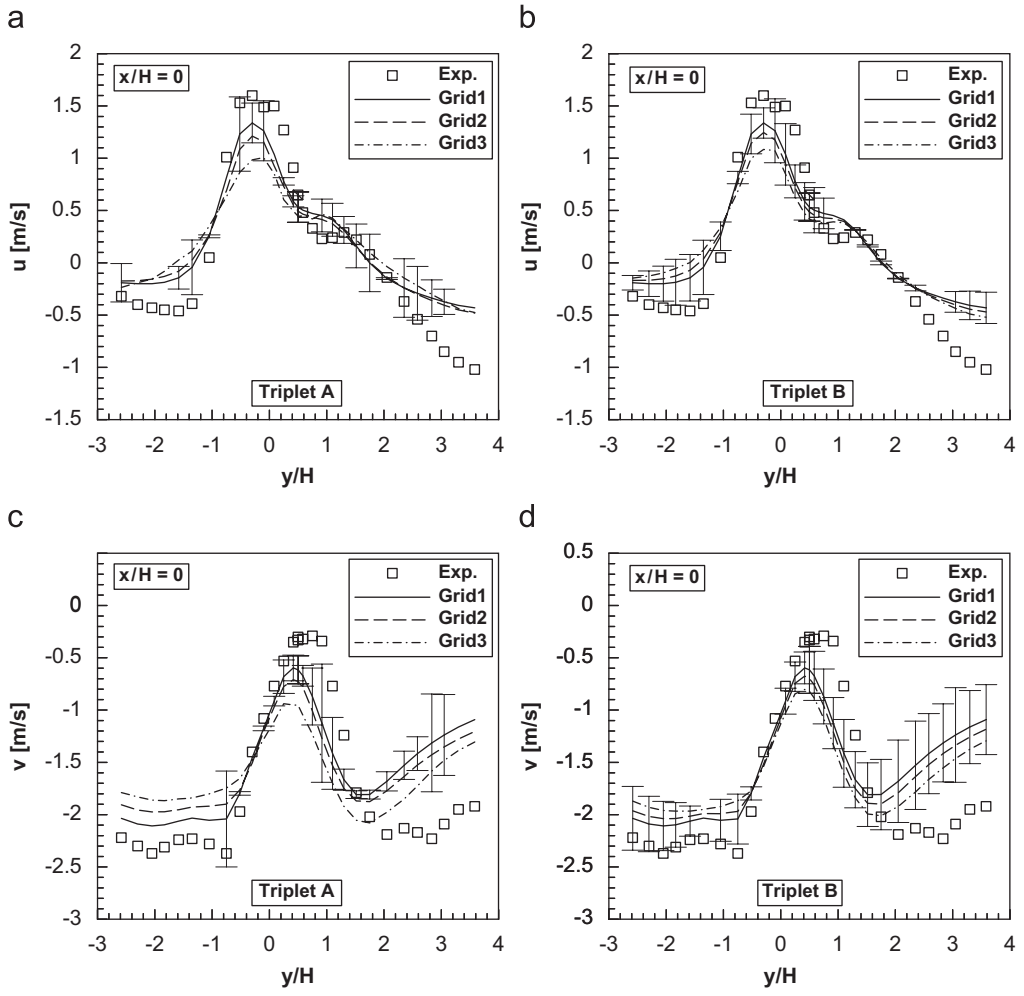

Fig. 5. Velocity distribution at $z/H = 0.5$ and $x/H = 0$ with error bars on the fine mesh, where error band estimates were possible: (a) u velocity for triplet A, (b) u velocity for triplet B, (c) v velocity for triplet A and (d) v velocity for triplet B.

both triplets yield roughly the same results with $\langle p \rangle$ lying in the range expected from the formal order of accuracy, see Section 4. Finally the average error band of the results on the fine grid, $\pm \langle U_1 \rangle$, and its root mean square value, $U_{1,\mathrm{rms}}$, are given. Both are computed from the results for conditions I–IV being fulfilled and are normalized by the maximum magnitude of the corresponding variable. The smallest average error bands are obtained for the u component, with triplet B yielding always smaller values than A, presumably again due to the fact that the coarse grid of triplet A does not yield results which are in the asymptotic range.

The substantially different solution obtained on the coarse grid of triplet A can also be seen in Figs. 5 and 6, where the computed velocity distributions are shown at two locations together with the error bars on the fine mesh. In Fig. 5 results for the u and the v component are shown at $z/H = 0.5$ and $x/H = 0$. Error bars are only plotted at those locations where the generalized Richardson extrapolation did not diverge. For both velocity components the solutions obtained with triplet B show a much nicer grid convergence as the results obtained with triplet A. Therefore also more positions contain error bars. Concerning the magnitude of the error bars the results from both triplets are comparable, showing that this approach yields robust results for the present case.

Contrary to this the corresponding results for the w component at $x/H = 0$ and $y/H = -1$, displayed in Fig. 6, show quite a different behaviour. There the error bars resulting from triplet B are substantially smaller than the error bars from triplet A. These larger error bars, however, correctly reflect the fact that the solution changes for triplet A are larger than the ones for triplet B.

Another result from Figs. 5 and 6 is that the fine grid solution does not necessarily show a better agreement with the experimental data than the solutions on the coarser grids. While in Fig. 5 the u and v velocity components of the fine grid solution are in closer agreement with the measurements for approximately $y/H \leqslant 2$, the disagreement increases with grid refinement for $y/H > 2$. For the w component shown in Fig. 6 the behaviour is

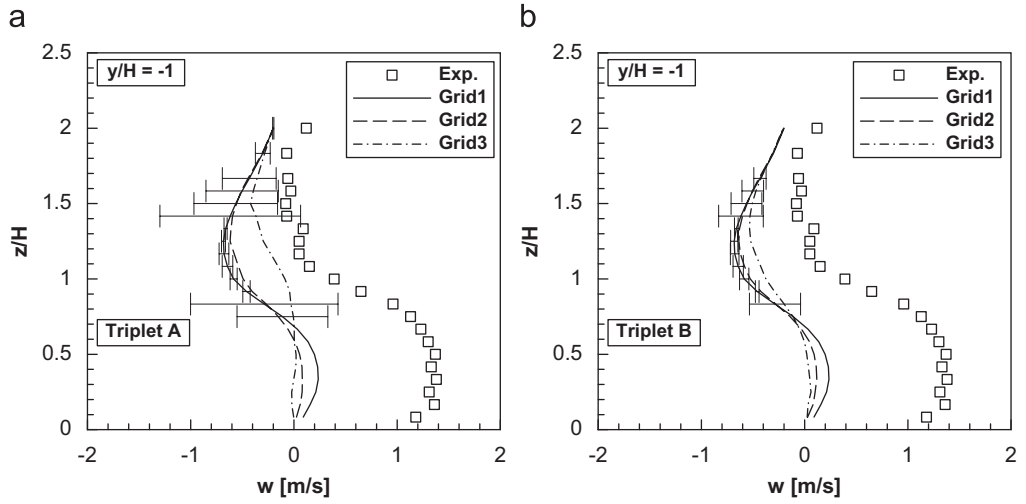

Fig. 6. Velocity distribution of w component at $y/H = -1$ and $x/H = 0$ with error bars on the fine mesh, where error band estimates were possible: (a) triplet A and (b) triplet B.

similar with better agreement below $z/H \approx 0.8$ and worse agreement above. For the evaluation of these results it is necessary to recapitulate that the numerical solutions mainly contain two sources of errors if the error from incomplete iterative convergence can be neglected, like in the present case. One error source is the turbulence model and the other source is the spatial discretisation error. If these errors have different signs they can partly compensate each other. With grid refinement the spatial discretisation error is reduced even though the estimated error bars in Figs. 5 and 6 are partly still quite large. The results for the velocity components shown in Figs. 5 and 6 therefore indicate that the standard k–ε turbulence model fails in accurately predicting the flow that enters the street intersection from the positive y/H-direction, while it is able to reproduce the recirculation region for $y/H \leqslant -1$. This was already shown by Franke and Frank (2005) with a detailed comparison of the experimental and numerical flow fields in the measurement planes at $z/H = 0.5$ and $y/H = -1$.

6. Conclusions

Generalized Richardson extrapolation as proposed by Eça and Hoekstra (2002, 2004) has been applied to the flow across an asymmetric street intersection to study the applicability of this approach to flow predictions in urban areas. The estimates of the error bands obtained for the three mean velocity components at the measurement positions do not depend strongly on the different grid triplets that have been used. The grid triplet A with constant refinement ratio suffers from the fact that the solution on the coarse grid is not in the asymptotic range. Grid triplet B has a substantially finer coarse mesh. Due to the non-constant refinement ratio, however, an iterative solution for the observed order of accuracy p is necessary, which increases the percentage of positions where no error estimate is possible. But still at approximately 70% of the measurement locations estimates for the error band are possible with triplet B, which is only slightly less than for triplet A. Whether the reduced average error band of triplet B is caused by the smaller number of locations with error band estimates, or by the better convergence properties of the finer grids is currently analysed. Additionally, the least squares approach recommended by Eça and Hoekstra (2002, 2004) due to its improved robustness will be applied with the available solutions from the five grids.

From the results presented here it can be concluded that the application of generalized Richardson extrapolation with grid triplets seems to be feasible for the prediction of mean velocities, at least in street intersections. Even the usage of a very coarse mesh is correctly reflected by larger error bars. Whether this approach is in general robust enough must be tested in the future by its application to more complex urban flow fields.

Acknowledgement

We gratefully acknowledge the partial support of this work by the German Research Foundation (DFG).

References

Blocken, B., Stathopoulos, T., Carmeliet, J., 2007. CFD simulation of the atmospheric boundary layer: wall function problems. Atmosph. Environ. 41, 238–252.

Cadafalch, J., Pérez-Segarra, C.D., Cònsul, R., Oliva, A., 2002. Verification of finite volume computations on steady-state fluid flow and heat transfer. J. Fluids Eng. 124, 11–21.

Eça, L., Hoekstra, M., 2002. An evaluation of verification procedures for CFD applications. In: Proceedings of the 24th Symposium on Naval Hydrodynamics, Fukuoka, 2002. 〈http://darwin.nap.edu/books/NI000511/html/568.html〉.

Eça, L., Hoekstra, M., 2004. A verification exercise for two 2-D steady incompressible turbulent flows. In: Neittaanmäki, P., Rossi, T., Majava, K., Pironneau, O. (Eds.), Proceedings of the ECCOMAS 2004, Jyväskylä.

FLUENT, 2003. FLUENT V6.1 User's Guide. Fluent Inc., Lebanon, New Hampshire.

Franke, J., Frank, W., 2005. Numerical simulation of the flow across an asymmetric street intersection. In: Náprstek, J., Pirner, M. (Eds.), Proceedings of the Fourth European–African Conference on Wind Engineering (EACWE4), Paper #138. Czech Technical University, Prague.

Franke, J., Frank, W., 2006. Application of Richardson extrapolation to the prediction of the flow field around building models. In: Proceedings of the Fourth International Symposium on Computational Wind Engineering (CWE2006), Yokohama, Japan, pp. 121–124.

Franke, J., Hirsch, C., Jensen, A.G., Krüs, H.W., Schatzmann, M., Westbury, P.S., Miles, S.D., Wisse, J.A., Wright, N.G., 2004. Recommendations on the use of CFD in wind engineering. In: van Beek, J.P.A.J. (Ed.), Proceedings of the International Conference on Urban Wind Engineering and Building Aerodynamics: COST C14—Impact of Wind and Storm on City life and Built Environment, C.1.1–C.1.11. Von Karman Institute for Fluid Dynamics, Rhode-Saint-Genèse.

Hargreaves, D.M., Wright, N.G., 2007. On the use of the k–ε model in commercial CFD software to model the neutral atmospheric boundary layer. J. Wind Eng. Ind. Aerodyn. 95, 355–369.

Leitl, B., 2000. Validation data for microscale dispersion modelling. EUROTRAC Newsletter 22, 28–32. 〈http://www.mi.uni-hamburg.de/CEDVAL-Validation-Data.427.0.html〉.

Oberkampf, W.L., Trucano, T.G., Hirsch, C., 2004. Verification, validation, and predictive capability in computational engineering and physics. Appl. Mech. Rev. 57, 345–384.

Richards, P.J., Hoxey, R.P., 1993. Appropriate boundary conditions for computational wind engineering models using the k–ε model. J. Wind Eng. Ind. Aerodyn. 46&47, 145–153.

Richardson, L.F., 1910. The approximate arithmetical solution by finite differences of physical problems involving differential equations with an application to the stresses in a masonry dam. Trans. Roy. Soc. Lond. Ser. A 210, 307–357.

Richardson, L.F., 1927. The deferred approach to the limit. Trans. Roy. Soc. Lond. Ser. A 226, 229–361.

Roache, P.J., 1994. Perspective: a method for uniform reporting of grid refinement studies. J. Fluids Eng. 116, 405–413.

Roache, P.J., 1998. Verification and Validation in Computational Science and Engineering. Hermosa, Albuquerque.

Roy, C.J., 2003. Grid convergence error analysis for mixed-order numerical schemes. AIAA J. 41, 595–604.

Roy, C.J., 2005. Review of code and solution verification procedures for computational simulation. J. Comput. Phys. 205, 131–156.